Journal of Computational Physics 229 (2010) 1558–1572

Contents lists available at ScienceDirect

Journal of Computational Physics

journal homepage: www.elsevier.com/locate/jcp

Induced electric current-based formulation in computations of low magnetic Reynolds number magnetohydrodynamic flows

S. Smolentsev [a,*], S. Cuevas [b], A. Beltrán [b]

[a] Mechanical and Aerospace Engineering Department, University of California, Los Angeles, 44-114 Engineering IV, Los Angeles, CA 90095-1597, USA
[b] Centro de Investigación en Energía, Universidad Nacional Autónoma de México, A.P. 34, Temixco, Morelos 62580, Mexico

ARTICLE INFO

Article history:
Received 9 June 2009
Received in revised form 23 October 2009
Accepted 26 October 2009
Available online 10 November 2009

Keywords:
Computational magnetohydrodynamics
High Hartmann number flows
Induced electric current

ABSTRACT

We use the induced electric current as the main electromagnetic variable to compute low magnetic Reynolds number magnetohydrodynamic (MHD) flows. The equation for the induced electric current is derived by taking the curl of the induction equation and using Ampère's law. Boundary conditions on the induced electric current are derived at the interface between the liquid and the thin conducting wall by considering the current loop closing in the wall and the adjacent liquid. These boundary conditions at the liquid–solid interface include the Robin boundary condition for the wall-normal component of the current and an additional equation for the wall potential to compute the tangential current component. The suggested formulation (denominated *j*-formulation) is applied to three common types of MHD wall-bounded flows by implementing the finite-difference technique: (i) high Hartmann number fully developed flows in a rectangular duct with conducting walls; (ii) quasi-two-dimensional duct flow in the entry into a magnet; and (iii) flow past a magnetic obstacle. Comparisons have been performed against the traditional formulation based on the induced magnetic field (*B*-formulation), demonstrating very good agreement.

Published by Elsevier Inc.

1. Introduction

High performance computing aimed at modeling magnetohydrodynamic (MHD) phenomena is a powerful method for studying complex liquid metal (LM) flows under non-uniform strong magnetic fields in many practical applications related to fusion reactors and metallurgy. Currently, much consideration is given to the development of new models and computer codes for MHD flows in a strong magnetic field for both open [1] and closed [2] duct flows as applied to LM cooling of the so-called plasma facing components of a fusion-power reactor. The starting point in such computations is the mathematical model, whose selection is influenced by the choice of flow/electromagnetic variables. Ordinary flows of incompressible fluids can be modeled with the Navier–Stokes equations written in various forms [3] based on the usage of primitive variables, i.e. velocity and pressure ($\mathbf{V}, P$); as well as vorticity (ω) and the stream function (ψ) (in 2-D flows); and vorticity–velocity or vector potential–vorticity. In the case of MHD flows, the governing equations include an additional set of equations, derived from the Maxwell equations, which in turn can be formulated in different ways. We can refer to several formulations of considerable use that implement the electric scalar (φ) or magnetic vector ($\mathbf{A}$) potential, as well as the magnetic field ($\mathbf{B}$) [4]. Other formulations based on the current vector potential ($\mathbf{T}$) or some combinations of the above quantities, for instance $\mathbf{A} - \varphi$, are also in a general use but mostly applied to calculations of eddy currents in a solid conductor [5]. Attempts on

* Corresponding author. Tel.: +1 310 794 5366; fax: +1 310 825 2599.
E-mail address: sergey@fusion.ucla.edu (S. Smolentsev).

0021-9991/$ - see front matter Published by Elsevier Inc.
doi:10.1016/j.jcp.2009.10.044

implementation of a formulation making use of the induced electric current as the main electromagnetic variable are relatively recent and still limited to a few classes of MHD problems. The so-called velocity–current formulation, in which the induced electric current is used as the principal electromagnetic field variable and the electric potential plays the role of a Lagrange multiplier associated with the current density, was first introduced in [6] and further elaborated in [7,8] for a class of stationary MHD problems. As stressed in [6], the current-based formulation avoids some disadvantages specific to the traditional velocity–magnetic field formulation. The important point to stress here is that modeling ordinary or MHD flows involves the freedom to chose a proper set of dependent variables. For a particular MHD flow problem, selecting one or another set of electromagnetic variables in combination with a proper numerical technique can result in a higher accuracy and faster convergence. Vice versa an inappropriate choice can lead to unphysical results as well as poor or no convergence at all. The choice of the electromagnetic variables can also affect the size and the shape of the integration domain and the way in which the boundary conditions are formulated that ultimately affects the computation cost. In the present paper, we elaborate a formulation, which similarly to studies in [6–8] makes use of the induced electric current but unlike the variational approach introduced in the abovementioned studies, implements the finite-different technique. By doing this, a governing equation for the induced electric current is derived by taking the curl of the induction equation and using Ampère's law. The suggested formulation can be used in computations not only steady but also time-dependent MHD flows. Additionally, "thin conducting wall" boundary conditions for the induced electric current are derived assuming that the thickness of the flow-bounding solid wall is significantly smaller than the characteristic flow dimension so that the electric current entering the wall from the liquid flows in the wall almost tangentially. The suggested formulation does not require computations of the electric potential in the flow region but an additional equation for the wall potential has to be solved at the liquid–solid interface to compute the tangential component of the induced current at the interface. The wall-normal current component at the interface is described with the Robin boundary condition. In this way, the derived equation for the induced electric current, the boundary conditions for the tangential and wall-normal current components along with the flow equations and proper conditions on the velocity components form a closed problem.

Typically, LM MHD flows in various applications are characterized by three dimensionless parameters: the Hartmann number ($Ha = B_0 L\sqrt{\sigma/\rho\nu}$), the Reynolds number ($Re = U_0 L/\nu$), and the magnetic Reynolds number ($Re_m = \mu\sigma U_0 L$). Here, B_0, L and U_0 are the characteristic magnetic field, flow dimension and velocity; while μ, σ, ρ and ν are the magnetic permeability, electrical conductivity, density and kinematic viscosity of the fluid, correspondingly. Hartmann number squared gives an estimate of the ratio of magnetic to viscous forces, while Re_m (when small) estimates the ratio of induced to applied magnetic field. In most applications involving LM MHD flows at industrial or laboratory scales, Re_m is much less than unity. Historically, the main challenge in modeling MHD wall-bounded flows is related to the need for fine resolution of MHD boundary layers that appear at the walls perpendicular to the applied magnetic field, known as Hartmann layers, whose thickness scales as $1/Ha$. In the fusion applications, the Hartmann number can be as high as 10^3–10^4, indicating the existence of very thin Hartmann layers. The small thickness of the Hartmann layer is, however, not the only limitation in advancing to higher Ha. In practice, computing high Hartmann number flows is also complicated by the fact that any local numerical error, for instance that in the Hartmann layers, will spread over the whole flow domain due to tight coupling between the flow and electromagnetic variables, distorting the computed flow field at a very short timescale. In the last two decades, many MHD computations were performed for duct flows (see e.g. [9–14]), but almost all of them are limited to $Ha \approx 10^2$. For example, in the widely cited study by Sterl [11], finite-volume 2-D and 3-D computations of MHD flows in rectangular ducts were conducted for both constant and space-varying magnetic fields with a maximum value of Ha of only 100 in the 3-D case. Such a limitation can be explained by the use of Ohm's law and the electric potential, which were implemented in all studies cited above. Namely, Ohm's law states that at low magnetic Reynolds numbers, the induced electric current $\mathbf{j}$ is given by

$$\mathbf{j} = \sigma(-\nabla\varphi + \mathbf{V}\times\mathbf{B}). \tag{1}$$

In typical LM MHD flows exhibiting Hartmann layers, the two terms on the right-hand side of Eq. (1) are of the same order, while the induced electric current is smaller by a factor of $1/Ha$. In this situation, small errors in computations of the electric potential or the velocity field may result in unacceptably high errors in $\mathbf{j}$, limiting the computations to relatively low Ha. In such situations (if special measures are not taken), the induced electric current path is not closed in the computational domain [12]. It appears that a numerical technique that does not fully compensate this kind of errors is impractical. Using higher accuracy schemes, finer meshes or double precision computations will probably extend the computations to higher values of Ha but will not solve the problem in principle. Fortunately, the problem of high Hartmann number computations can be mitigated in two ways. First, new numerical schemes, still based on the φ-formulation, can be developed, in which the error associated with Ohm's law is self-compensated. Such an approach has recently been demonstrated in [15] allowing accurate computations of MHD flows in a rectangular duct for Ha as high as 10^4. The second approach assumes abandoning the φ-formulation in favor of another formulation, which does not base the calculation of currents on Ohm's law. A well-known formulation of that type, which uses the magnetic field as the electromagnetic variable, involves Ampère's law to compute the electric current:

$$\mathbf{j} = \frac{1}{\mu}\nabla\times\mathbf{B}. \tag{2}$$

From the point of view of numerical computations, relation (2) has some advantage over (1). Namely, even with some inaccuracy in computing the magnetic induction field $\mathbf{B}$, the electric current calculated with (2), by virtue of the vector identity

$\nabla \cdot (\nabla \times \mathbf{B}) = 0$, is always divergence-free (not counting the numerical error from approximation of the ∇ operator). Physically this means that the induced electric current paths are closed. In contrast, in the φ-formulation, a divergence-free current is not directly guaranteed since $\nabla \cdot \mathbf{j} = -\nabla \cdot (\sigma \nabla \varphi) + \nabla \cdot (\sigma \mathbf{V} \times \mathbf{B})$, that involves an error associated with the numerical method by which the governing equations were solved. That is why the current paths are not necessarily closed. Unlike the electric potential, using the magnetic field in 2-D calculations for fully developed [16] or developing flows [17], without taking any special measures to provide $\nabla \cdot \mathbf{j} = 0$, has demonstrated no restrictions on *Ha*. The computations show a very good convergence for both conducting and insulating walls at *Ha* as high as 10^3–10^4. However, extending this approach to general 3-D flows, where all three components of the induced magnetic field are present, is seriously complicated by several technical challenges. One of them is the need to formulate the boundary conditions on the magnetic field at a considerable distance from the flow domain, where the induced magnetic field vanishes. This also may require implementation of the internal boundary conditions on the magnetic field at the interfaces, such as between the liquid and the flow containing walls. Another problem is satisfying the condition $\nabla \cdot \mathbf{B} = 0$ (see also discussion in Section 2) when solving the induction equation. To our knowledge, there are no studies that address adequately all these issues simultaneously.

The main goal of the present paper is to introduce a formulation for wall-bounded MHD flows, which can be used along with traditional φ- and *B*-formulations. This formulation is based on the induced electric current as an electromagnetic variable (*j*-formulation). From a numerical point of view, the *j*-formulation promises some advantages compared to the other two formulations. First of all, similarly to the *B*-formulation, it does not use Ohm's law to calculate electric currents, and thus is free from the specific errors associated with Ohm's law, so that the induced electric current path computed with the *j*-formulation is always closed within the computational domain. Second, the boundary conditions on the induced electric current at the liquid–solid interface can be formulated as the "thin conducting wall" approximation so that no computations are needed in the solid wall and also in the adjacent exterior domain. The apparent disadvantage compared to the φ-formulation is, however, a need to solve three scalar equations for the current components compared to only one equation for the electric potential. Solving three scalar equations is, nevertheless, generally required when using the *B*-formulation. The new formulation is introduced in Section 2, including derivations of boundary conditions at the interface between the liquid and the solid wall. The next sections illustrate the application of the *j*-formulation to three particular MHD flows: (i) fully developed flows in a rectangular duct with thin conducting walls (Section 3), (ii) quasi-two-dimensional MHD flow at the entry to a magnet (Section 4), and (iii) MHD flow past a magnetic obstacle (Section 5). The main conclusions on this *j*-formulation are presented in Section 6.

2. Mathematical formulation based on the induced electric current and thin conducting wall boundary conditions

We start our considerations with the well-known formulation based on the magnetic field as the main electromagnetic variable by introducing the induction and flow equations first. The desirable counterpart for the electromagnetic equation in the *j*-formulation can then be obtained by taking curl of the induction equation. If $\mathbf{V}$ is the velocity vector in the fluid, and ∇ denotes the gradient operator of 3-D space, the governing flow equations can be formulated in terms of the primitive variables as follows (see e.g. [4]):

$$\frac{\partial \mathbf{V}}{\partial t} + (\mathbf{V} \cdot \nabla)\mathbf{V} = -\frac{1}{\rho}\nabla P + \nu \nabla^2 \mathbf{V} + \frac{1}{\rho}\nabla \cdot \left(\frac{\mathbf{BB}}{\mu} - \frac{B^2}{2\mu}\mathbf{I}\right), \tag{3}$$

$$\nabla \cdot \mathbf{V} = 0. \tag{4}$$

The last term on the right-hand side of the momentum equation, which expresses the effect of the electromagnetic field on the fluid, is written in the conservative form as the divergence of the Maxwell stress tensor, where $\mathbf{I}$ is the unit tensor. Providing the condition $\nabla \cdot \mathbf{B} = 0$ is not violated, this term can also be written in a non-conservative form as $\mathbf{j} \times \mathbf{B}/\rho$. In turn, the induction equation describing the distribution of the magnetic field is written in the full form as follows:

$$\frac{\partial \mathbf{B}}{\partial t} = \eta \nabla^2 \mathbf{B} + \nabla \times (\mathbf{V} \times \mathbf{B}) - \eta \nabla (\nabla \cdot \mathbf{B}), \tag{5}$$

where $\eta = 1/\mu\sigma$ is the magnetic diffusivity. The last term in this equation becomes zero providing the magnetic field is preserved solenoidal. However, the accumulation of the numerical errors in the course of numerical computations may violate this condition resulting in numerical divergence or/and unphysical solutions. That is why the term including $\nabla \cdot \mathbf{B}$ on the right-hand side of the induction equation is often retained. It should be noted that the above formulation is widely used in many numerical computations of various MHD flows in plasma physics applications where the magnetic Reynolds number can be as high as 10^8. In these conditions the effects associated with the propagation of the Alfvén waves and other MHD effects typical to fusion or astrophysical plasmas are of special importance and the conservative form of the momentum equation (3) becomes preferable to ensure the required accuracy. However, there can be some penalty for using the conservative form, as shown by Brackbill and Barnes [18]. Namely, small violation of $\nabla \cdot \mathbf{B} = 0$ may result in unphysical solutions that appear as a force parallel to the magnetic field, that is $(\nabla \cdot \mathbf{B})\mathbf{B}/\rho\mu$, which tends to distort the velocity field in time. In turn, the velocity field distortions may cause further violation of the $\nabla \cdot \mathbf{B} = 0$ condition. Once the cause of the problem was understood in the recent past, a number of cleaning procedures ensuring $\nabla \cdot \mathbf{B} = 0$ in the three-dimensional case was

successfully developed (see e.g. already mentioned article by Brackbill and Barns [18], as well as references in the paper by Yagi et al. [19]).

In the present study, we restrict our considerations to incompressible electrically conducting viscous liquids (such as LMs) with constant material properties in a steady magnetic field under conditions when the inductionless approximation holds, i.e. $Re_m \ll 1$. In this case, the total magnetic field can be decomposed into the applied and induced parts, namely,

$$\mathbf{B} = \mathbf{B}^0 + \mathbf{B}^i. \tag{6}$$

such that $\mathbf{B}^i \ll \mathbf{B}^0$ and the contribution of $\mathbf{B}^i$ to the Lorentz force term in the momentum equation can be neglected. A number of small terms in the induction equation, all of the order of magnitude of Re_m, including the unsteady term, can also be neglected. In addition, unlike the plasma physics applications, all terms that include $\nabla \cdot \mathbf{B}$ in both the momentum and induction equations are dropped. The latter seems to be justified as the Alfvén waves typical to plasma physics applications are quickly damped, so that using the momentum equation in the conservative form is not required. Although small errors associated with the condition $\nabla \cdot \mathbf{B} = 0$ are still possible, these errors do not go beyond the usual round-off and their appearance does not cause catastrophic changes in the solution as happens in the case of $Re_m \gg 1$, where the numerical errors are unacceptably high due to their amplification by very large magnetic Reynolds numbers. Writing the electromagnetic term on the right-hand side as just $\mathbf{j} \times \mathbf{B}^0$ also eliminates in the numerical solution the unphysical Lorentz force component parallel to the magnetic field. Finally the momentum and induction equation written in the classic quasi-static low magnetic Reynolds number approximation (see e.g. [4]) take the following form:

$$\frac{\partial \mathbf{V}}{\partial t} + (\mathbf{V} \cdot \nabla)\mathbf{V} = -\frac{1}{\rho}\nabla P + \nu \nabla^2 \mathbf{V} + \frac{1}{\rho}\mathbf{j} \times \mathbf{B}^0, \tag{7}$$

$$0 = \eta \nabla^2 \mathbf{B}^i + \mathbf{S}_B, \tag{8}$$

where $\mathbf{S}_B = \nabla \times (\mathbf{V} \times \mathbf{B}^0) = (\mathbf{B}^0 \cdot \nabla)\mathbf{V} - (\mathbf{V} \cdot \nabla)\mathbf{B}^0$ is the source term. The governing equation for $\mathbf{j}$ can now be obtained by applying the curl operator to the induction equation (8):

$$0 = \eta \nabla^2 \mathbf{j} + \mathbf{S}_j, \tag{9}$$

where the new source term, $\mathbf{S}_j$, is given by

$$\mathbf{S}_j = \frac{1}{\mu}\nabla \times \mathbf{S}_B. \tag{10}$$

Similarly to the electric potential, the electric current is distributed only within a conducting region that includes liquid and conducting walls. No calculations of $\mathbf{j}$ are needed in the outside space or within a non-conducting wall. In the case of a thin conducting wall, the current in the wall is mostly tangential and almost does not vary across the wall. This leads us to use approximate boundary conditions at the boundaries of the flow domain. In doing so, the calculations of electric currents can be reduced to the flow domain only.

To derive the boundary conditions for the electric current at the interface with a thin electrically conducting wall, let us consider a small section of the solid wall adjacent to the liquid (Fig. 1). The current generated in the liquid enters the wall through the liquid–wall interface Γ and then turns in the wall in a tangential direction. The continuity equation for the electric current in this region can be written as

$$\frac{\partial j_n}{\partial n} = -\nabla_\tau \cdot \mathbf{j}_\tau, \tag{11}$$

where subindexes n and τ stand for normal and tangential components, respectively. Integrating Eq. (11) across the wall, assuming that the normal component of the current at the outer surface of the wall is zero, yields at the fluid–wall interface Γ

$$j_n(\Gamma) = -\nabla_\tau \cdot (t_w \mathbf{j}_{\tau w}), \tag{12}$$

where $\mathbf{j}_{\tau w}$ is the current in the wall, which to the leading order of approximation does not vary across the wall, and t_w is the wall thickness. Due to continuity of the tangential component of the electric field across the interface, we have

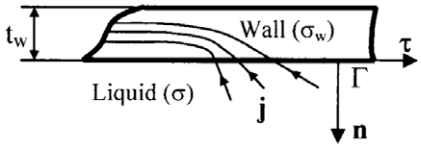

Fig. 1. Sketch of the electric current distribution near and within a thin conducting wall.

$$\frac{\mathbf{j}_\tau(\Gamma)}{\sigma} = \frac{\mathbf{j}_{\tau w}}{\sigma_w}. \tag{13}$$

Substituting $\mathbf{j}_{\tau w}$ from (13) into (12) and using the continuity equation for the electric current, results in the following boundary condition for the normal component of the current at the wall

$$j_n(\Gamma) = \frac{t_w\sigma_w}{\sigma}\frac{\partial j_n(\Gamma)}{\partial n} - \left(\nabla_\tau \frac{t_w\sigma_w}{\sigma}\right) j_\tau(\Gamma), \tag{14}$$

or in a dimensionless form assuming that t_w and σ_w are constant

$$\tilde{j_n}(\Gamma) - c_w \frac{\partial \tilde{j_n}(\Gamma)}{\partial \tilde{n}} = 0,$$

where $c = \sigma_w t/\sigma L$ is the wall conductance ratio. This boundary condition is identical in form to that of the induced magnetic field in the thin conducting wall approximation in fully developed flows [20]. As for the boundary condition for $\mathbf{j}_\tau$, it can be obtained by introducing the wall potential, φ_w, such that

$$\mathbf{j}_{\tau w} = -\sigma_w \nabla_\tau \varphi_w. \tag{15}$$

After substitution of (15) into (12) one can obtain the following second-order partial differential equation for the wall potential

$$j_n(\Gamma) = \nabla_\tau \cdot (t_w\sigma_w \nabla_\tau \varphi_w). \tag{16}$$

Providing Eq. (16) is solved, the electric current in the wall can be calculated using (15) and then the distribution of the tangential current at the liquid–wall interface, $\mathbf{j}_\tau(\Gamma)$, can be found using (13). In the special case of non-conducting walls, the boundary condition (14) is reduced to $j_n = 0$.

It is easy to see that the suggested j-formulation can be considered as a trade-off between the electric potential and induced magnetic field formulations. Similarly to the φ-formulation, the domain of integration does not include the non-conducting exterior. Moreover, even though the flow-bounding walls are electrically conducting, the computations within the wall region are not needed (providing that the usage of thin conducting wall boundary conditions can be justified). Similarly to the B-formulation, it does not rely on Ohm's law as a way to calculate the electric current in the flow domain. Although the formulation uses the electric potential in the wall area, the problem encountered with the φ-formulation in the flow domain does not arise, since Ohm's law in the wall is reduced to $\mathbf{j} = -\sigma\nabla\varphi$. However, the number of equations to be solved in comparison with the B-formulation is increased by one due to the need of computing the wall potential. In what follows, numerical aspects of implementation of the new formulation and new boundary conditions are illustrated by three particular MHD flows.

3. Fully developed flow in a rectangular duct

As a first example, we consider here a laminar flow of an electrically conducting liquid through a thin-walled straight rectangular duct (Fig. 2) in a transverse uniform magnetic field B_z^0. We assume the flow to be fully developed, so that all variables are independent of the axial coordinate, except for the pressure, which is a linear function of x. Under these conditions,

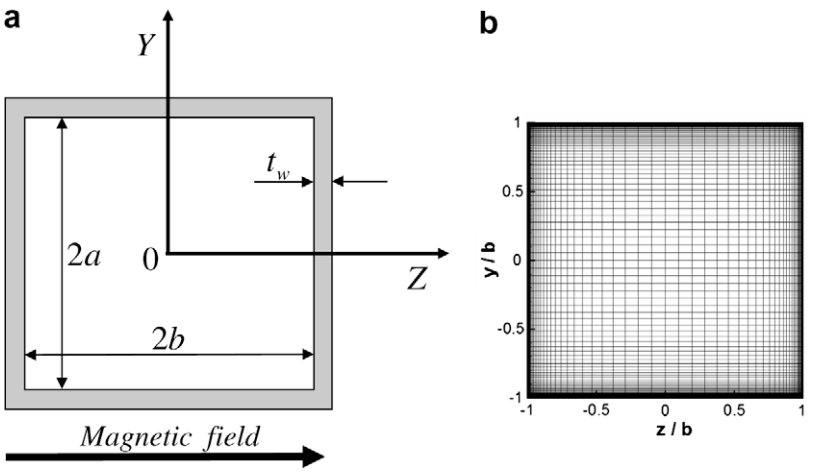

Fig. 2. Sketch of the cross-sectional area of the rectangular duct with thin conducting walls in the problem for a fully developed flow (a), and example of the computational mesh in the flow domain (b).

the vector equations (7) and (9) can be reduced to three scalar equations written in terms of the axial velocity U and two cross-sectional electric current components j_z and j_y as follows:

$$\nu\left(\frac{\partial^2 U}{\partial z^2}+\frac{\partial^2 U}{\partial y^2}\right)-\frac{1}{\rho}\frac{dP}{dx}+\frac{1}{\rho}j_y B_z^0=0, \tag{17}$$

$$\frac{\partial^2 j_z}{\partial z^2}+\frac{\partial^2 j_z}{\partial y^2}-\sigma B_z^0\frac{\partial^2 U}{\partial z\,\partial y}=0, \tag{18}$$

$$\frac{\partial^2 j_y}{\partial z^2}+\frac{\partial^2 j_y}{\partial y^2}+\sigma B_z^0\frac{\partial^2 U}{\partial z^2}=0. \tag{19}$$

Note that only one electric current component j_y is required to compute the Lorentz force. However, both equations (18) and (19) have to be solved because of the coupling between j_z and j_y through the boundary conditions. In the thin wall approximation, the boundary conditions on the electric current include the Robin-type condition for the wall-normal component of the electric current and an additional equation for the wall potential, which is used to compute the tangential component:

$$z=\pm b: j_z\pm t_w\frac{\sigma_w}{\sigma}\frac{\partial j_z}{\partial z}=0,\quad \frac{d^2\varphi_w}{dy^2}=\mp\frac{j_z}{t_w\sigma_w},\quad j_y=-\sigma\frac{d\varphi_w}{dy},\quad U=0, \tag{20}$$

$$y=\pm a: j_y\pm t_w\frac{\sigma_w}{\sigma}\frac{\partial j_y}{\partial y}=0,\quad \frac{d^2\varphi_w}{dz^2}=\mp\frac{j_y}{t_w\sigma_w},\quad j_z=-\sigma\frac{d\varphi_w}{dz},\quad U=0. \tag{21}$$

It is more convenient to rewrite Eqs. (17)–(19) and boundary conditions (20) and (21) in a dimensionless form by using proper scales: $[z]=[y]=b$ as a length scale, $[U]=b^2\nu^{-1}\rho^{-1}(-dP/dx)$ as a velocity scale, $[j_z]=[j_y]=\sigma[U]B_z^0$ as a scale for the induced electric current, and $[\varphi]=b[U]B_z^0$ as a scale for the wall potential. Then, the equations and boundary conditions take the following form:

$$\frac{\partial^2\widetilde{U}}{\partial\tilde{z}^2}+\frac{\partial^2\widetilde{U}}{\partial\tilde{y}^2}+1+Ha\tilde{j}_y=0, \tag{22}$$

$$\frac{\partial^2\tilde{j}_z}{\partial\tilde{z}^2}+\frac{\partial^2\tilde{j}_z}{\partial\tilde{y}^2}-Ha\frac{\partial^2\widetilde{U}}{\partial\tilde{z}\,\partial\tilde{y}}=0, \tag{23}$$

$$\frac{\partial^2\tilde{j}_y}{\partial\tilde{z}^2}+\frac{\partial^2\tilde{j}_y}{\partial\tilde{y}^2}+Ha\frac{\partial^2\widetilde{U}}{\partial\tilde{z}^2}=0, \tag{24}$$

$$\tilde{z}=\pm1: \tilde{j}_z\pm c_w\frac{\partial\tilde{j}_z}{\partial\tilde{z}}=0,\quad \frac{d^2\tilde{\varphi}_w}{d\tilde{y}^2}=\mp\frac{\tilde{j}_z}{c_w},\quad \tilde{j}_y=-\frac{d\tilde{\varphi}_w}{d\tilde{y}},\quad \widetilde{U}=0, \tag{25}$$

$$\tilde{y}=\pm a/b: \tilde{j}_y\pm c_w\frac{\partial\tilde{j}_y}{\partial\tilde{y}}=0,\quad \frac{d^2\tilde{\varphi}_w}{d\tilde{z}^2}=\mp\frac{\tilde{j}_y}{c_w},\quad \tilde{j}_z=-\frac{d\tilde{\varphi}_w}{d\tilde{z}},\quad \widetilde{U}=0. \tag{26}$$

Eqs. (22)–(24) and boundary conditions (25) and (26) are approximated using a finite-difference technique on a co-located non-uniform mesh (U, j_z, and j_y are defined at the same location), which clusters grid points within the Hartmann layers and within the side layers at the duct walls parallel to the magnetic field (Fig. 2(b)). Optimal ratio between the number of grid points in the MHD boundary layers and that in the flow bulk is achieved by using a special stretching transformation for boundary layer type flows proposed by Roberts [21]. The three equations are solved iteratively until the steady-state solution is achieved using the ADI (alternative direction implicit) scheme [22]. The equation for the wall potential itself requires additional boundary conditions, which are chosen in such a way that $\tilde{\varphi}_w=0$ at $\tilde{y}=0$ and $d\tilde{\varphi}_w/d\tilde{z}=0$ at $\tilde{z}=0$ to account for symmetry. The equation for the wall potential is solved with a conventional tridiagonal solver. In doing so, the corners are treated as special points where the electric current in the wall turns under a right angle assuming $d\tilde{\varphi}_w/d\tilde{z}=d\tilde{\varphi}_w/d\tilde{y}$ at these points to assure current continuity.

Computations using the new formulation have been performed for high Hartmann number flows ($Ha=5000$) for a thin-walled square duct. The results are compared with the computations based on the well-tested B-formulation code [23] for $c_w=0.01$ ($\sigma_w=\sigma$, $t_w/b=0.01$). The B-formulation code solves the momentum and the induction equation in the domain that includes the flow and the electrically conducting wall. Both codes use the same non-uniform mesh in the flow domain of 101×101 grid points. In the computations based on the B-formulation, additional 75 grid points are added in the wall. Other details of the B-formulation code can be found in [23]. The two computations are in a very good agreement as seen in Fig. 3. In this figure the velocity is scaled with the mean bulk velocity U_m. The distribution of the wall potential is illustrated in Fig. 4(a) and the convergence of the iteration process using the j-formulation in Fig. 4(b), where the dimensionless flow rate $Q=\int\int\widetilde{U}\,d\tilde{z}\,d\tilde{y}$ is shown as a function of the iteration number N. The convergence demonstrates oscillating behavior. The convergence rate can be significantly improved by applying a special relaxation-like acceleration procedure similar to that used in [23]. However, the code acceleration is not amongst the main priorities of the current research, which mostly focuses

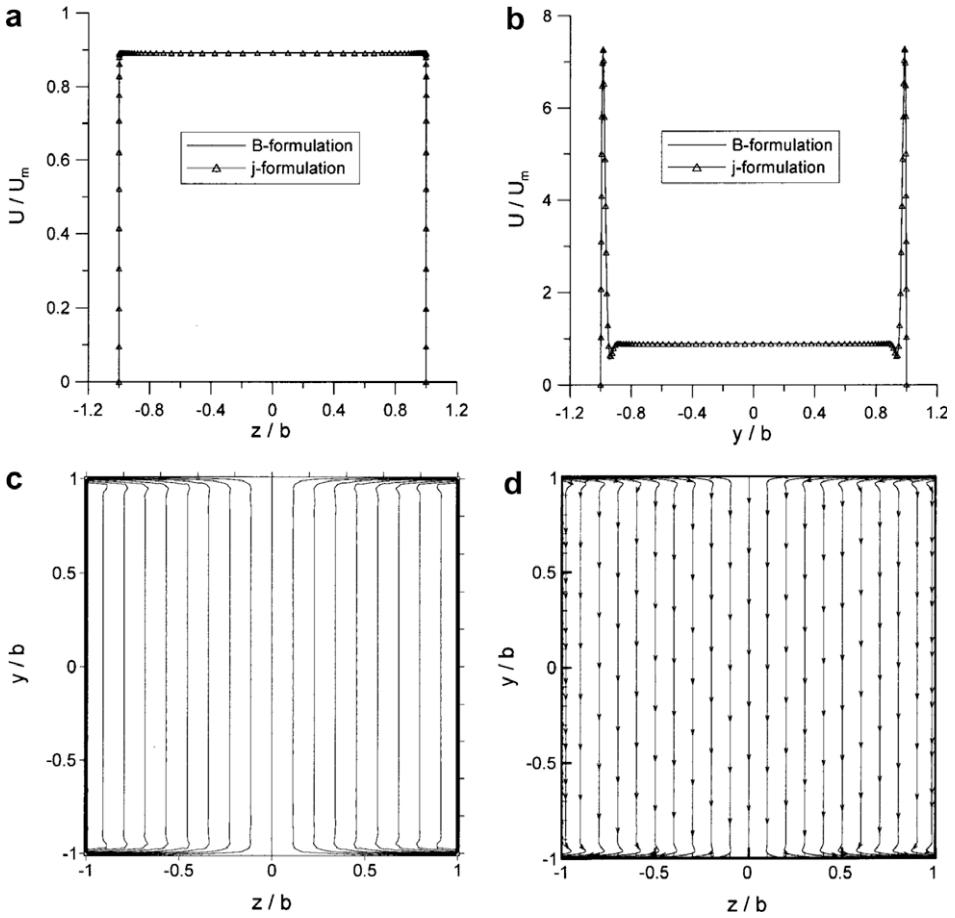

Fig. 3. Comparison between the *j*- and *B*-formulation for a fully developed flow in a square duct with thin electrically conducting walls at $Ha = 5000$ and $c_w = 0.01$: (a) velocity distribution along z axis at $y = 0$; (b) velocity distribution along y axis at $z = 0$; (c) induced magnetic field isolines (*B*-formulation); and (d) induced electric current tracers (*j*-formulation).

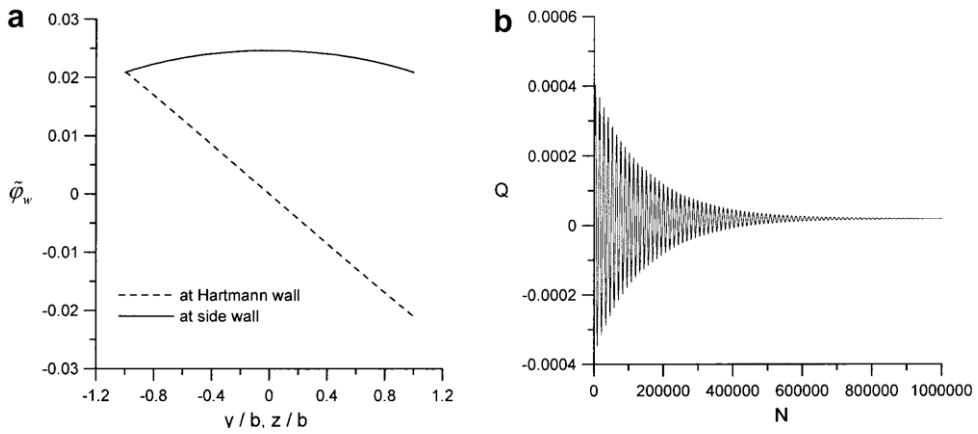

Fig. 4. Distribution of the wall potential (a) and convergence (b) in computations using *j*-formulation for $Ha = 5000$ and $c_w = 0.01$.

on the new formulation itself. Moreover, the computational time is from minutes to a few hours for *Ha* from hundreds to thousands, using a PC. The computational time using the *j*-formulation, is typically two to five times higher compared to the *B*-formulation as more iterations are usually required due to the need for the special procedure associated with the boundary conditions on the electric current as described above. More computational time is needed for higher *Ha*.

4. Duct flow at the entry to a magnet

Here, we apply the new formulation to computations of MHD duct flows in a so-called "fringing" magnetic field (Fig. 5). Unlike the flow in the previous example, the flow in a fringing magnetic field is developing as the electric current is induced not only in the cross-sectional but also in the axial planes. The following model for duct flows in a fringing magnetic field has been adopted from [24], where a number of novelties (for example, an explicit treatment of the current exchange mechanism between the cross-sectional and axial loops) were introduced. Here, we focus mostly on the numerical implementation of the *j*-formulation.

The reference flow has dimensions $2b$ in the field direction (z-direction) and $2a$ in the y-direction. Present considerations are limited to flows in a non-conducting duct with a small aspect ratio $\varepsilon = b/a < 1$, assuming also that the magnet dimension along the y-axis is much larger than the corresponding duct dimension $2a$, so that the applied magnetic field in the flow domain is y-independent, changing in the axial direction from zero at $x = -\infty$ to some constant value B_0. Under these conditions, the distribution of the applied magnetic field associated with the entry into a magnet, which to the leading order of magnitude satisfies the magnetostatic equations, as derived in [24], has the following form:

$$\left.\begin{aligned} B_x &= z\partial_x B_* + O(\varepsilon_m^3 B_0),\\ B_y &= O(\varepsilon_m^3 B_0),\\ B_z &= B_*(x,y) - \tfrac{z^2}{2}(\partial_x^2 B_* + \partial_y^2 B_*) + O(\varepsilon_m^4 B_0). \end{aligned}\right\} \tag{27}$$

where ε_m is the magnet aspect ratio similar to the duct aspect ratio ε. All magnetic field components can be expressed through the function $B^*(x)$ given below in a parametric form, which describes the axial variations of the applied magnetic field within the symmetry plane of the magnet as follows:

$$\beta = \frac{B_*(x)}{B_0} = \frac{1}{s}, \quad \tilde{x} = \frac{x}{a} = -\frac{2\varepsilon}{\pi}\left[s + \frac{1}{2}\log\left(\frac{s-1}{s+1}\right)\right] + C. \tag{28}$$

In what follows the determination of the arbitrary constant entering (28) is based on the condition $\beta = 0.5$ at $\tilde{x} = 0$.

Under the assumption $\varepsilon < 1$, the reference flow in a strong fringing magnetic field is essentially 2-D ($U = U(x,y)$, $V = V(x,y)$, $W = 0$), except for the thin Hartmann layers at the walls $z = \pm b$, where the velocity field depends on all three coordinates. The induced electric current, at the same time, is 3-D as both cross-sectional and axial currents are present. The quasi-two-dimensional (Q2D) nature of the flow allows for the reduction of the original set of three-dimensional equations to a Q2D form by integrating the original equations in the z-direction analytically. The resulting equations can then be expressed in terms of the vorticity $\omega(x,y)$ ($\omega = \partial V/\partial x - \partial U/\partial y$), stream function $\psi(x,y)$ ($U = \partial\psi/\partial y$, $V = -\partial\psi/\partial x$), and the induced electric current components $j_x(x,y)$ and $j_y(x,y)$ (see [24] for details), all associated with the flow in the core, as follows:

$$\frac{\partial\tilde{\omega}}{\partial\tilde{t}} + \tilde{U}\frac{\partial\tilde{\omega}}{\partial\tilde{x}} + \tilde{V}\frac{\partial\tilde{\omega}}{\partial\tilde{y}} = \frac{1}{Re}\left(\frac{\partial^2\tilde{\omega}}{\partial\tilde{x}^2} + \frac{\partial^2\tilde{\omega}}{\partial\tilde{y}^2}\right) - \frac{Ha}{\varepsilon^2 Re}\beta\tilde{\omega} - \frac{Ha^2}{\varepsilon^2 Re}\frac{d\beta}{d\tilde{x}}\tilde{j}_x, \tag{29}$$

$$\frac{\partial^2\tilde{\psi}}{\partial\tilde{x}^2} + \frac{\partial^2\tilde{\psi}}{\partial\tilde{y}^2} = -\tilde{\omega}, \tag{30}$$

$$\frac{\partial^2\tilde{j}_x}{\partial\tilde{x}^2} + \frac{\partial^2\tilde{j}_x}{\partial\tilde{y}^2} = \frac{\partial}{\partial\tilde{y}}\left(\tilde{U}\frac{d\beta}{d\tilde{x}}\right) + \frac{1}{Ha}\frac{\partial\tilde{\omega}}{\partial\tilde{x}}, \tag{31}$$

$$\frac{\partial^2\tilde{j}_y}{\partial\tilde{x}^2} + \frac{\partial^2\tilde{j}_y}{\partial\tilde{y}^2} = -\frac{\partial}{\partial\tilde{x}}\left(\tilde{U}\frac{d\beta}{d\tilde{x}}\right) + \frac{1}{Ha}\frac{\partial\tilde{\omega}}{\partial\tilde{y}}. \tag{32}$$

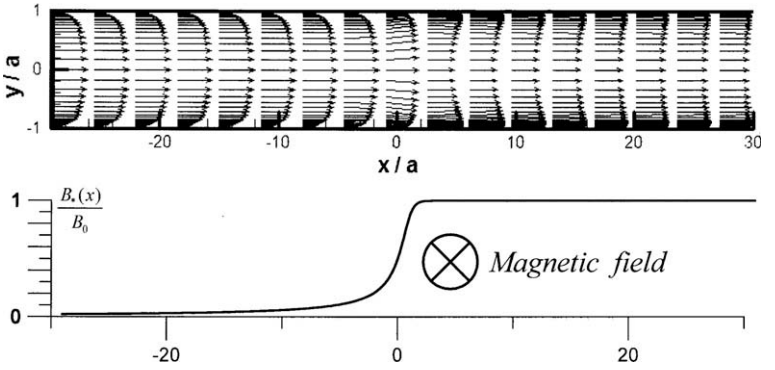

Fig. 5. Sketch of the reference duct flow in a fringing magnetic field, showing the mid-plane of the duct, typical velocity vectors, and the distribution of the transverse component of the applied magnetic field.

Additionally, the third component of the current $\tilde{j}_z$ is treated analytically to give the following relation:

$$\tilde{j}_z = -\frac{1}{Ha}\tilde{\omega}\tilde{z}. \tag{33}$$

Unlike $\tilde{j}_x$ and $\tilde{j}_y$,$\tilde{j}_z$ depends on all three coordinates. All current components are interrelated through the continuity equation:

$$\frac{\partial \tilde{j}_x}{\partial \tilde{x}} + \frac{\partial \tilde{j}_y}{\partial \tilde{y}} + \frac{\partial \tilde{j}_z}{\partial \tilde{z}} = 0. \tag{34}$$

Eqs. (29)–(34) are written in a dimensionless form using the mean bulk velocity U_m as the velocity scale, half-width of the duct a in the direction perpendicular to the magnetic field direction as a characteristic linear dimension, and $\sigma U_m B_0$ as a scale for the induced electric current. The Reynolds number is constructed using the dimension a, while the Hartmann number definition is based on the Hartmann length b. The boundary conditions at the walls $\tilde{y} = \pm 1$ for the induced electric current for a non-conducting duct are $\tilde{j}_y = 0$ and $\partial \tilde{j}_x/\partial \tilde{y} = 0$. The boundary conditions at the flow inlet/outlet are of Neumann type, $\partial/\partial \tilde{x} = 0$, as the flow far upstream or downstream from the fringing field is fully developed. The introduction of the wall potential as described in Section 2 and also illustrated in Section 3 is not necessary in this particular case since much more simple boundary conditions shown above can directly be applied. Eq. (32) is in fact not used in the numerical code and given here for completeness. When computing the electric current, the $\tilde{j}_x$-component is computed first using Eq. (31), and then, $\tilde{j}_y$ is computed using the continuity Eq. (34) and relation (33).

Eqs. (29)–(34) are approximated using a finite-difference technique on a co-located mesh similar to a standard $\psi - \omega$ technique (see e.g. [3]). The computational mesh clusters the grid points near the walls $\tilde{y} = \pm 1$ to resolve the side layers. The whole problem is solved by advancing in time, until a steady-state solution is achieved. The vorticity equation at each time step and that of the induced electric current are solved using the TDMA (Tridiagonal Matrix Algorithm) method in both coordinate directions. The convective terms in the vorticity equation are approximated with the central-difference scheme, which is known to be dissipation free. The elliptic equation for the stream function, whose solution usually takes most of the computational time, is solved with the cosine fast Fourier transform (cos FFT) in the x-direction and the tridiagonal algorithm in the y-direction. Using the FFT technique limits the computational grid in the axial direction to a uniform spacing, but is more effective compared with much slower and less accurate relaxation techniques. Using the cos FFT in $\tilde{x}$ also requires the inlet/outlet boundaries to be positioned far enough from the fringing field region, so that the Neumann boundary condition is allowed. In this way, the typical calculation domain is 40–60 units long (longer domains for higher Re). Satisfactory resolution is achieved by using 512 or 1024 grid points in the axial direction and 201 points in the other direction. The numerical tests include grid sensitivity tests, and comparisons with the analytical solution for a fully developed flow. The comparisons demonstrate agreement in local values between the analytical and the numerical results as good as four digits.

Computed flow results are shown in Fig. 6 for two sets of flow parameters: Ha = 200, Re = 100,000, ε = 0.2 and Ha = 2000, Re = 500, ε = 0.2, which represent inertial and inertialess flow regimes, correspondingly. In both cases, a characteristic feature of the velocity profile is a slow variation in the upstream region and then fast formation of high velocity near-wall jets and associated M-shaped velocity profile once the liquid enters the magnet zone. In the inertialess regime, the M-shaped velocity profile relaxes very fast to the well-known Shercliff-type flow with a uniform core and two symmetric side layers with the thickness scaling as $1/\sqrt{Ha}$, while in the inertial regime the M-shaped velocity profile persists over a long downstream region. These observations are in a good qualitative agreement with experimental data for a flow in a slotted duct in a fringing magnetic field [25]. Quantitative comparisons with the experimental data are, however, not possible because of limited information on experimental conditions presented in [25]. Fig. 6 also shows the distribution of the induced electric current in the form of three streamtracer rakes plotted at different locations along the x-axis. Clearly, there are two electric current loops: cross-sectional and axial. In the cross-sectional loop, the currents are closed through the Hartmann layers at the walls $z = \pm b$ and the side layers at the walls $y = \pm a$, while in the axial loop, closing occurs in the flow bulk in the $x - y$ planes. The three-dimensional current distribution in the fringing field region reduces to a well-known two-dimensional distribution downstream of the magnet entry zone as the flow becomes fully developed. Details of the current distribution are however different between inertial and inertialess flows. Notice that in spite of high Reynolds number (high interaction number) in the inertial flow and two distinctive inflection points in the velocity profile, the computed flow remains stable. This seems to have a physical rather than a numerical reason as recent experimental data [26] demonstrate damping turbulence pulsations at the entry to a magnet. On the other hand, there is a theoretical argument (see e.g. [27]), which explains the flow stabilization with high dissipation losses that occur once the pulsating flow crosses the so-called characteristic surfaces [28] associated with the non-uniform magnetic field.

5. Flow past a magnetic obstacle

In the examples presented in Sections 3 and 4, we have considered time-independent MHD flows. We now apply the new formulation to a recently studied flow that can display either steady or time-dependent behavior [29,30]. The problem consists of a uniform shallow flow, bounded in z-direction by two insulating walls, past a strongly localized non-homogeneous magnetic field that occupies only a small fraction of the total flow domain (Fig. 7). The motion of the fluid through the localized field induces electric currents that interact with the applied magnetic field producing a Lorentz force that opposes the

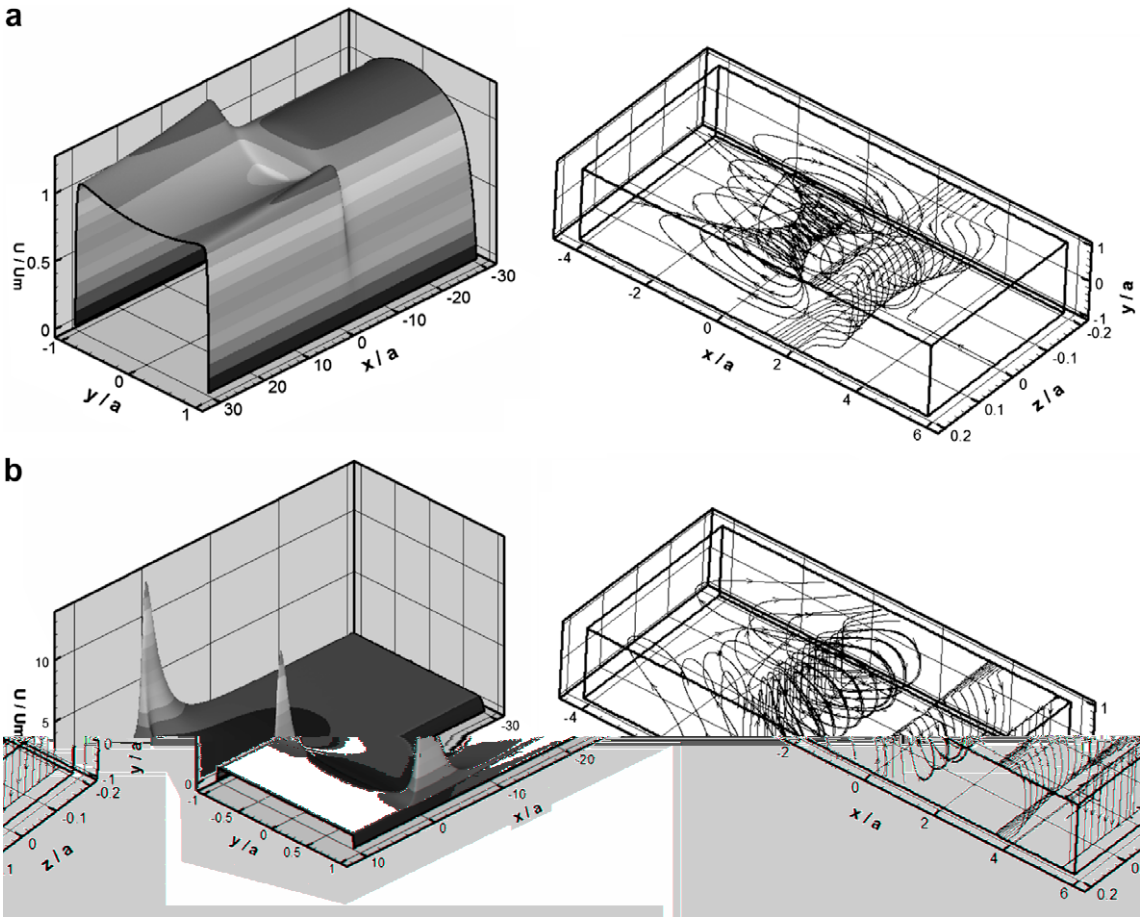

Fig. 6. Axial velocity (left) and 3-D induced electric current (right) in the flow in a fringing magnetic field computed with *j*-formulation. (a) Inertial regime $Ha = 200$, $Re = 100{,}000$ and $\varepsilon = 0.2$. (b) Inertialess regime: $Ha = 2000$, $Re = 500$, $\varepsilon = 0.2$. Closing currents in the Hartmann layer is not seen directly because the Q2D model takes the Hartmann layers into account implicitly.

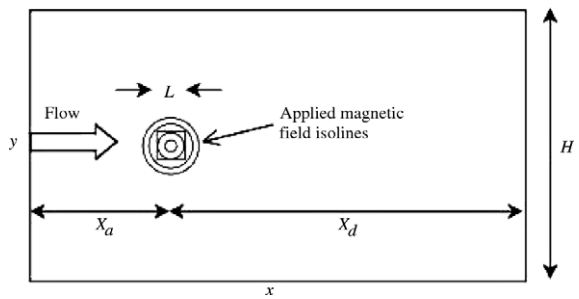

Fig. 7. Flow configuration and basic geometrical parameters for the flow past a magnetic obstacle.

oncoming flow. In fact, this non-homogeneous magnetic field acts as an obstacle for the flow and, according to the physical conditions, different flow patterns can arise that resemble, in some aspects, the ones observed in flows past bluff bodies. Originally, this flow was studied numerically using the *B*-formulation in [29], where the term *magnetic obstacle* was coined to recall the analogy with solid obstacles.

As common in shallow flow calculations, we use a Q2D approach assuming that the transport of momentum in the wall-normal direction is mainly diffusive. Similarly to the flow discussed in Section 4, it is possible to reduce the three-dimensional equations to a Q2D form by integrating them analytically along the wall-normal *z*-direction [29]. In this way, the friction effects due to the flow-bounding walls are considered through a linear term that accounts for the friction inside and outside the applied magnetic field. The applied field is created by two magnetized insulated square surfaces embedded in

the walls, for which an explicit analytical expression is available [31,29]. Within the Q2D approximation, it is necessary to consider only the contribution of the dominant component of the field in the z-direction, $B_z^0 = B_z^0(x,y)$. The dimensionless governing equations can then be expressed in terms of the velocity, pressure and electric current density in the form

$$\frac{\partial \widetilde{U}}{\partial \tilde{x}} + \frac{\partial \widetilde{V}}{\partial \tilde{y}} = 0, \tag{35}$$

$$\frac{\partial \widetilde{U}}{\partial \tilde{t}} + \widetilde{U}\frac{\partial \widetilde{U}}{\partial \tilde{x}} + \widetilde{V}\frac{\partial \widetilde{U}}{\partial \tilde{y}} = -\frac{\partial \widetilde{P}}{\partial \tilde{x}} + \frac{1}{Re}\left(\frac{\partial^2 \widetilde{U}}{\partial \tilde{x}^2} + \frac{\partial^2 \widetilde{U}}{\partial \tilde{y}^2}\right) - \frac{\widetilde{U}}{\tilde{\tau}} + \frac{Ha^2}{Re}\tilde{j}_y \widetilde{B}_z^0, \tag{36}$$

$$\frac{\partial \widetilde{V}}{\partial \tilde{t}} + \widetilde{U}\frac{\partial \widetilde{V}}{\partial \tilde{x}} + \widetilde{V}\frac{\partial \widetilde{V}}{\partial \tilde{y}} = -\frac{\partial \widetilde{P}}{\partial \tilde{y}} + \frac{1}{Re}\left(\frac{\partial^2 \widetilde{V}}{\partial \tilde{x}^2} + \frac{\partial^2 \widetilde{V}}{\partial \tilde{y}^2}\right) - \frac{\widetilde{V}}{\tilde{\tau}} - \frac{Ha^2}{Re}\tilde{j}_x \widetilde{B}_z^0, \tag{37}$$

$$\frac{\partial^2 \tilde{j}_x}{\partial \tilde{x}^2} + \frac{\partial^2 \tilde{j}_x}{\partial \tilde{y}^2} = \frac{\partial^2}{\partial \tilde{x}\partial \tilde{y}}(\widetilde{U}\widetilde{B}_z^0) + \frac{\partial^2}{\partial \tilde{y}^2}(\widetilde{V}\widetilde{B}_z^0), \tag{38}$$

$$\frac{\partial^2 \tilde{j}_y}{\partial \tilde{x}^2} + \frac{\partial^2 \tilde{j}_y}{\partial \tilde{y}^2} = \frac{\partial^2}{\partial \tilde{x}\partial \tilde{y}}(\widetilde{V}\widetilde{B}_z^0) + \frac{\partial^2}{\partial \tilde{x}^2}(\widetilde{U}\widetilde{B}_z^0), \tag{39}$$

where we use the uniform velocity U_0 as a velocity scale, the side length of the magnetized plate L as a characteristic length scale, the maximum field strength B_{max} as a magnetic field scale, and $\sigma U_0 B_{max}$ as a scale for the induced currents. In Eqs. (36) and (37), dimensionless parameter $\tilde{\tau}$ characterizes the friction effect due to the flow-bounding walls (for definition of $\tilde{\tau}$, see [29]). Similarly to the study performed in [29], in the present numerical calculations we consider conditions where inertial effects dominate over the wall friction. A rectangular domain of 35×20 measured in units of the characteristic length L, is considered. A uniform flow in the x-direction is prescribed at the inlet, namely, $\widetilde{U} = 1, \widetilde{V} = 0, \tilde{j}_x = \tilde{j}_x = 0$. The center of the magnetic obstacle, that is the point of maximum magnetic field strength, is located in the midline axis 10 units downstream from the inlet. At the outlet, Neumann conditions are used, $\partial \widetilde{U}/\partial \tilde{x} = \partial \widetilde{V}/\partial \tilde{x} = \partial \tilde{j}_x/\partial \tilde{x} = \partial \tilde{j}_y/\partial \tilde{x} = 0$. At the lateral boundaries, symmetry-type conditions simulating a frictionless wall were imposed, $\partial \widetilde{U}/\partial \tilde{y} = \widetilde{V} = 0$. Finally, we assume that at the lateral boundaries the induced current components satisfy $\partial \tilde{j}_y/\partial \tilde{y} = \tilde{j}_x = 0$. Since j_y and j_x are defined at the same location as velocity components $\widetilde{U}$ and $\widetilde{V}$ (see Fig. 8), these are also symmetry-type conditions for the current. In fact, the width of the domain in the y-direction is chosen long enough so that the induced current is negligible at lateral boundaries. As initial condition, the fluid was assumed to be at rest.

A finite-difference method on an orthogonal equidistant grid of 213×201 is used to solve governing equations (35)–(39) under the specified initial and boundary conditions. A spatial discretization of second-order accuracy is done on a staggered grid (Fig. 8), while the Euler method is used for time discretization. The velocity component U and current density component j_y are defined at the center of the vertical surfaces of the computational cell, while components V and j_x are placed at the horizontal surfaces. In turn, the pressure and the applied magnetic field are both defined at the center of the computational cell. Diffusive terms are discretized using central differences. For convective terms, a mixture of central differences and the donor-cell discretization, as suggested in [32], is implemented. The standard time-marching procedure described in [33], is extended to include Eqs. (38) and (39). The time discretization of the momentum equation is explicit in the velocities and implicit in the pressure. It has been determined that a time increment of 0.005 for the main iteration loop guarantees accurate computations. In all cases, the electric current is closed as seen directly in the figures and also indicated by the divergence of the induced current, which does not exceed 10^{-4}.

Depending on the governing parameters Re and Ha, that determine inertial and magnetic braking effects, the flow can display steady patterns with or without vortices or a wavy wake and even a periodic vortex shedding. For particular sets of Re and Ha, results computed with the new formulation based on the induced electric current are compared with those using the B-formulation [29] that utilizes the same mesh and time increment. Fig. 9(a) shows the induced magnetic field isolines in the neighborhood of the magnetic obstacle, calculated with the B-formulation for the case $Re = 100$ and

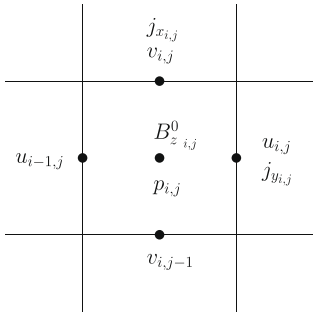

Fig. 8. Computational cell used in the computations for the flow past a magnetic obstacle with j-formulation.

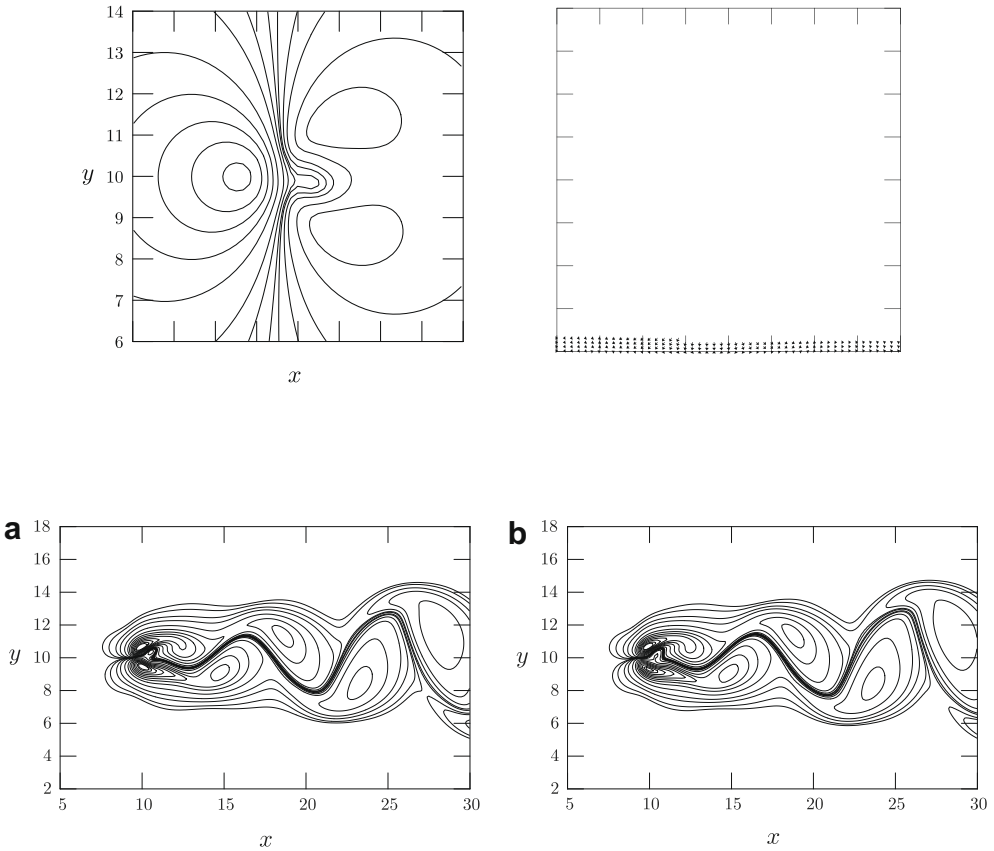

Fig. 10. Vorticity isolines in the flow past a magnetic obstacle for *Re* = 100 and *Ha* = 50. (a) Calculated with *B*-formulation. (b) Calculated with *j*-formulation.

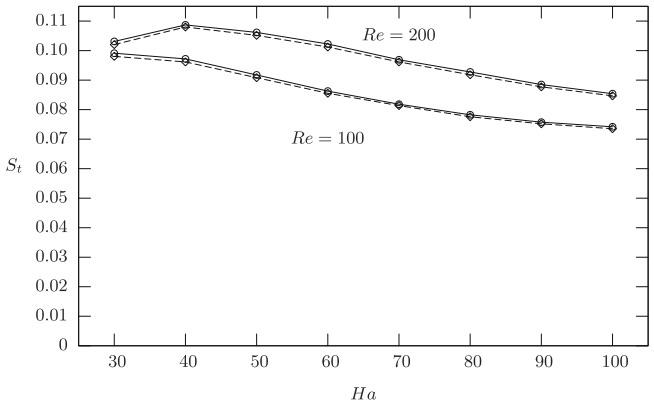

Fig. 12. Strouhal number versus Hartmann number computed with two formulations. *B*-formulation: continuous line. *j*-formulation: dotted line.

Ha = 50. The isolines correspond to the current paths since the induced field serves as a stream function for the current density. In turn, Fig. 9(b) shows the corresponding current density field calculated with the *j*-formulation. The current distribution displayed in both figures match very well. For these parameter values, the wake of the magnetic obstacle presents a periodic vortex shedding so that a von Kármán street is formed, as clearly observed in Fig. 10(a and b) where the vorticity isolines calculated with the *B*- and *j*-formulation, respectively, are shown in the flow domain.

Fig. 11(a) shows the comparison for velocity component $\widetilde{U}$ as a function of the axial coordinate for a steady flow (*Re* = 100, *Ha* = 10), while Fig. 11(b) presents the same comparison for a time-dependent flow (*Re* = 100, *Ha* = 50).

Fig. 11(c and d) shows, respectively, the current component $\tilde{j}_x$ in the axial direction and the vorticity as a function of time for the same unsteady case at *Re* = 100 and *Ha* = 50. Note that the component $\tilde{j}_x$ displays a very regular behavior that incidentally is very similar to the one found in the steady flow. On the other hand, the variation of vorticity with time clearly reflects the periodic behavior of the flow. However, it should be mentioned, that transient states are slightly different for each formulation. In fact, the *j*-formulation reaches a steady-state faster than the *B*-formulation. In general, it can be observed that even in a time-dependent flow, computations performed with both formulations are in a fair agreement. A good match between results computed with the two formulations for unsteady flows is also seen in Fig. 12 where a global parameter, namely, the dimensionless frequency associated with vortex shedding in the wake (the Strouhal number, $St = fL/U_0$) is computed for two Reynolds numbers as a function of *Ha*. Although the results are close, the *j*-formulation gives slightly lower frequencies compared to the other one. This might be related to differences in approximation of Eqs. (38) and (39) for the electric current and the induction equation in the *B*-formulation.

6. Conclusions

We have introduced a formulation utilizing the induced electric current as an electromagnetic variable as a possible approach for computing wall-bounded MHD flows, which can be used along with canonical formulations based on the electric potential and induced magnetic field [Eq. (9)] . Additionally to the flow equations, this formulation includes an equation for the induced electric current and boundary conditions [Eqs. (14)–(16)] that adopt the well-known "thin conducting wall approximation". In the new boundary conditions, the wall-normal component of the induced electric current at the wall is described by the Robin-type relation, which includes the wall conductance ratio c_w as a coefficient. Corresponding boundary condition can be directly incorporated into any standard elliptic solver. The computation of the tangential component of the induced electric current at the wall is less straightforward and generally requires solving an additional equation for the wall potential, which has also been derived in the paper [Eq. (16)]. Compared to the velocity-current formulation in its current form (see [6–8]), the present one is more general allowing for computations of unsteady flows and more suited for matching problems, when the flow is bounded by thin electrically conducting walls. Compared to the traditional φ- and *B*-formulation, the new one introduces some advantages. First of wall, it does not rely on Ohm's law for computing the induced electric current in the flow domain and thus is free from the potential numerical error that may result in electric current discontinuity, which is often observed in high Hartmann number computations when the φ-formulation is used. Second, it does not require computations in the wall and in the outer space as needed when the *B*-formulation is used for 3-D flows. The disadvantage compared to the φ-formulation is the need to solve three (in 3-D flows) or two (in 2-D flows) equations for the current components compared to only one for the electric potential. Compared to the *B*-formulation, extra computational time may be needed due to additional computations associated with the wall potential. However, total benefits of the new formulation will depend on a concrete physical problem and can be affected by many parameters, including the flow geometry, wall conductivity, applied magnetic field distribution, etc.

A number of examples have been given to illustrate the implementation of the new formulation and also to test several standard numerical techniques in combination with the newly-derived equations for the induced electric current and thin

conducting wall boundary conditions. Three flow cases considered in the paper address special types of flows, such as fully developed flows in a conducting duct in a strong magnetic field, developing steady flows in a non-uniform magnetic field, and unsteady flows past a localized magnetic field zone (magnetic obstacle). The standard computational techniques, such as classical stream function-vorticity approach as well as one based on the usage of primitive variables, including staggered and co-located meshes, have been adapted to account for computing the induced electric currents. These computations have been compared (where possible) against the classical *B*-formulation, demonstrating very good agreement. Taken together, all these make us to believe that the suggested new formulation is potentially a very attractive tool for computations of high Hartmann number MHD flows. However, in spite of many potential advantages, the present approach and especially the associated numerical codes have similar limitations as analogous non-MHD codes. For example, increasing *Re* significantly in calculations of unsteady or developing flows may cause unphysical oscillations presumably related to the limit on the schematic Reynolds number. Nevertheless the ways of mitigating such problems are well described in the specialized literature (see e.g. [3]). No limitation has been determined on the Hartmann number providing a special care is taken on accurate resolution of the Hartmann and side layers.

Finally, we would like to stress that the new formulation has been introduced in the most general three-dimensional form, while the numerical examples in the paper are limited to a number of two-dimensional and quasi-two-dimensional flows. Such flows are, however, very typical in many MHD applications, e.g. in poloidal ducts of a liquid metal blanket. Therefore, the considered examples cover the broad class of practically important MHD problems. For all the examples we have not observed any violation of the charge conservation law $\nabla \cdot \mathbf{j} = 0$ as directly seen from the induced electric current distributions, where all induced currents are closed within the integration domain. Although $\nabla \cdot \mathbf{j} = 0$ is not satisfied precisely in the computations, the discrepancy is always within the usual computational errors, which can easily be controlled by changing the computational mesh or increasing the approximation order of the numerical schemes. If necessary, for essentially three-dimensional flows, cleaning procedures to ensure $\nabla \cdot \mathbf{j} = 0$ can also be added in analogy with the *B*-formulation.

Acknowledgments

S.S. acknowledges support through DOE Grant DE-FG02-86ER52123-A040. S.C. and A.B. acknowledge support from CONACYT through Project 59977 and a Ph.D. grant, respectively. A.B. also acknowledges support from the fusion group at UCLA during his research stay. We also wish to thank Dr. Leo Bühler for his useful discussions on the thin wall boundary conditions and Prof. René Moreau for his contribution to the development of a new model for flows in a fringing field used in this paper.

References

[1] M. Abdou, A. Ying, N. Morley, K. Gulec, S. Smolentsev, et al, On the exploration of innovative concepts for fusion chamber technology, APEX Interim Report Overview, Fusion Eng. Des. 54 (2001) 181–247.
[2] S. Smolentsev, N.B. Morley, M. Abdou, R. Munipalli, R. Moreau, Current approaches to modeling MHD flows in the dual coolant lead lithium blanket, Magnetohydrodynamics 42 (2006) 225–236.
[3] J.C. Tannehill, D.A. Anderson, R.H. Pletcher, Computational Fluid Mechanics and Heat Transfer, second ed., Taylor & Francis, 1997.
[4] R. Moreau, Magnetohydrodynamics, Kluwer Academic Publishers, Dordrecht/Boston/London, 1990.
[5] A. Krawczyk, J.A. Tegopoulos, Numerical Modelling of Eddy Currents, Clarendon Press, Oxford, 1993.
[6] A.J. Meir, Paul G. Schmidt, A velocity–current formulation for stationary MHD flows, Appl. Math. Comput. 65 (1994) 95–109.
[7] A.J. Meir, Paul G. Schmidt, Variational methods for stationary MHD flow under natural interface conditions, Nonlinear Anal. Theory Meth. Appl. 26 (1996) 659–689.
[8] A.J. Meir, Paul G. Schmidt, Analysis and numerical approximation of a stationary MHD flow problem with nonideal boundary, SIAM J. Numer. Anal. 36 (1999) 1304–1332.
[9] T.N. Aitov, A.I. Kalyutik, A.V. Tananaev, Numerical analysis of three-dimensional MHD flow in channel with abrupt change of cross-section, Magnetohydrodynamics 2 (1983) 223–229.
[10] C.N. Kim, M.A. Abdou, Numerical method for fluid flow and heat transfer in magnetohydrodynamic flow, Fusion Technol. 15 (1989) 1163–1168.
[11] A. Sterl, Numerical simulation of liquid–metal MHD flows in rectangular ducts, J. Fluid Mech. 216 (1990) 161–191.
[12] H. Araseki, S. Kotake, A self-correcting procedure for computational liquid metal magnetohydrodynamics, J. Comput. Phys. 110 (1994) 301–309.
[13] M.V. Myasnikov, S.Yu. Smolentsev, Numerical investigation of the velocity field deformation in an electrically conducting liquid passing a magnetic zone. Three-dimensional formulation, Magnetohydrodynamics 34 (1998) 272–279.
[14] L. Leboucher, Monotone scheme and boundary conditions for finite volume simulation of magnetohydrodynamic internal flows at high Hartmann number, J. Comput. Phys. 150 (1999) 181–198.
[15] M.-J. Ni, R. Munipalli, N.B. Morley, P. Huang, M. Abdou, A current density conservative scheme for incompressible MHD flows at a low magnetic Reynolds number. Part I: on a rectangular collocated grid system, J. Comput. Phys. 227 (2007) 174–204.
[16] S. Smolentsev, Mathematical models for magnetohydrodynamic flows in a fusion reactor blanket, Plasma Dev. Operat. 7 (1999) 231–241.
[17] S. Smolentsev, M. Abdou, Open-surface MHD flow over a curved wall in the 3-D thin-shear-layer approximation, Appl. Math. Model. 29 (2005) 215–234.
[18] J.U. Brackbill, D.C. Barnes, The effect of nonzero $\nabla \cdot B$ on the numerical solution of the magnetohydrodynamic equations, J. Comput. Phys. 35 (1980) 426–430.
[19] M. Yagi, K. Seki, Y. Matsumoto, Development of a magnetohydrodynamic simulation code satisfying the solenoidal magnetic field condition, Comput. Phys. Commun. 180 (2009) 1550–1557.
[20] J.A. Shercliff, The flow of conducting fluids in circular pipes under transverse magnetic fields, J. Fluid Mech. 6 (1956) 644–666.
[21] G.O. Roberts, Computational meshes for boundary layer problems, in: Proceedings of the Second International Conference on Numerical Methods in Fluid Dynamics, Lecture Notes on Physics, vol. 8, Springer-Verlag, New York, 1971, pp. 171–177.
[22] D.W. Peaceman, H.H. Rachford, The numerical solution of parabolic and elliptic differential equations, J. Soc. Ind. Appl. Math. 3 (1955) 577–590.
[23] S. Smolentsev, N. Morley, M. Abdou, Code development for analysis of MHD pressure drop reduction in a liquid metal blanket using insulation technique based on a fully developed flow model, Fusion Eng. Des. 73 (2005) 83–93.

[24] R. Moreau, S. Smolentsev, S. Cuevas, A refined theory of channel flows in a fringing field, in: Fifth International Symposium on Electromagnetic Processing of Materials, Sendai, Japan, 2006, pp. 133–138.
[25] A.V. Tananaev, Flows in Channels of MHD-Devices, Moscow, Atomizdat, 1979 (in Russian).
[26] O. Andreev O, Yu. Kolesnikov, A. Thess, Experimental study of liquid metal channel flow under the influence of a nonuniform magnetic field, Phys. Fluid 18 (2007) 065108.
[27] B. Knaepen, R. Moreau, Magnetohydrodynamic turbulence at low magnetic Reynolds number, Annu. Rev. Fluid Mech. 40 (2008) 25–45.
[28] A. Kulikovskii, Slow steady flows of a conducting fluid at high Hartmann number, Izv. Akad. Nauk SSSR. Mekh. Zhidk. Gaza 3 (1968) 3–10.
[29] S. Cuevas, S. Smolentsev, M. Abdou, On the flow past a magnetic obstacle, J. Fluid Mech. 553 (2006) 227–252.
[30] E.V. Votyakov, E. Zienecke, Y. Kolesnikov, Constrained flow around a magnetic obstacle, J. Fluid Mech. 610 (2008) 131–156.
[31] M. McCaig, Permanent Magnets in Theory and Practice, Wiley, New York, 1977.
[32] C. Hirt, B. Nichols, N. Romero, SOLA a numerical solution algorithm for transient fluid flows. Technical Report LA-5852, Los Alomos, NM: Los Alamos National Lab., 1975.
[33] M. Griebel, T. Dornseifer, T. Neunhoeffer, Numerical Simulation in Fluid Dynamics, SIAM, New York, 1998.